UCSF
UC San Francisco Electronic Theses and Dissertations

Title
Strategies in MR-guided focused ultrasound

Permalink
https://escholarship.org/uc/item/3jx5k7g2

Author
Tibrewala, Radhika

Publication Date
2017

Peer reviewed|Thesis/dissertation

eScholarship.org Powered by the California Digital Library
University of California

Strategies in MR-guided focused ultrasound

by

Radhika Tibrewala

THESIS

Submitted in partial satisfaction of the requirements for the degree of

MASTER OF SCIENCE

in

Biomedical Imaging

in the

GRADUATE DIVISION

of the

UNIVERSITY OF CALIFORNIA, SAN FRANCISCO

[redacted]

Acknowledgments

I would first like to thank my thesis advisor Dr.Viola Rieke of the Radiology Department at University of California San Francisco. Dr.Rieke had a monumental role in not only helping me efficiently shape and complete my project, but she gave me the time and guidance in order for me to actually learn the importance of the basics in MRI without which this project would not have been possible. Besides her guidance for this project, she was also a wonderful mentor who always had her office door open whenever I needed any advice in my project or my career goals. She let this paper be my own work, but always steered me in the right direction when I needed it.

I would also like to thank Dr.Eugene Ozhinsky of the Radiology Department at University of California San Francisco. Dr.Ozhinsky was the primary reason that I was to build the simulation. He very patiently helped me troubleshoot my problems every time I hit a road block. He also took the time out to run phantom experiments with me and teach me new and invaluable things. Most importantly, I would like to thank him for ingraining in me the importance of being meticulous and thorough with my code and always encouraging me to learn new ways to parallel process and handle big data sets, these are skills that I will build on and use for the rest of my academic and professional career, and he has equipped me with the zest to learn more in this field.

I would like to thank Dr.William Grissom of the Biomedical Engineering department at Vanderbilt University. He was willing to share his code which helped me get started on building my simulation.

I would like to acknowledge Dr.Matthew Bucknor and Dr.Chris Diederich of the Radiology and Radiation Oncology departments respectively at University of California San Francisco as members of my thesis committee. I am gratefully indebted to them for their comments and advice on my thesis defense and thesis.

Lastly, I would like to thank my sister for her continuous support after I moved to San Francisco. She was there for me throughout my researching and writing process.

Abstract

Purpose

To determine under-sampled k-space gradient echo trajectories for MR thermometry with PRF shift to increase acquisition speed while maintaining temperature accuracy.

Methods

A computer simulation was built and used to study the behaviour of temperature measurement errors as different lines of k-space were acquired. A fully acquired k-space was constructed from the information in the Bioheat Transfer Equation (BHTE), various k-space under-sampling schemes were employed and temperature maps were reconstructed using the PRF shift method as a basis. Temperature errors were calculated as the difference in the maximum temperature predicted by the BHTE and the maximum temperature measured by the under-sampled scheme.

Results

Under-sampled gradient echo keyhole trajectories showed promising results for making temperature measurements. Using 5 interleaves with a 63 keyhole size estimates temperature with only a 0.4% error while providing a 1.68x faster frame rate.

Conclusion

Gradient echo keyhole trajectories can be used to make temperature measurements for MR thermometry with PRF shift. This method can also be applied for shorter sonications and making temperature estimates for multiple slices.

Contents

1 Introduction **1**

1.1 Principles of MR-guided Focused Ultrasound 1

1.2 Applications of HIFU 1

1.3 Magnetic Resonance Thermometry 1

1.4 Proton Resonance Frequency 2

1.5 Pulse Sequences for MR Thermometry 3

1.6 Pennes Bioheat Transfer Equation 4

2 Methods **4**

2.1 Gradient Echo Keyhole and Trajectory Design 4

2.2 RTHawk Implementation 6

2.3 Phantom Data Acquisition 7

2.4 Mathematical Simulation Based on the Bioheat Transfer Equation 9

2.5 Under-sampling and Reconstruction Process 11

2.6 Synchronization 12

2.7 Reducing Sonication Time 13

2.8 Faster Frame Rate for Multiple Slices 13

3 Results **14**

3.1 Experimental Data 14

3.2 Mathematical Model 15

3.2.1 Low Frequency Data Only 16

3.2.2 Combination of High Frequency Data (Interleaved) and Low Frequency (keyhole) Data 17

3.2.3 Reducing Sonication Time 20

3.2.4 Selected Schemes for Multiple Slices 22

4 Discussion **23**

4.1 Experimental Data 23

4.2 Low-frequency Data Only 25

4.3 Combination of High Frequency Data (Interleaved) and Low Frequency Data 26

4.4 Limitations of Simulated Model 28

4.5 Future Directions 28

5 Conclusion **29**

References **30**

List of Tables

1 Examples of under-sampled schemes and corresponding acceleration factors . 6

2 Results of phantom experiments 14

3 Selected under-sampled schemes from low-frequency data only 16

4 Selected under-sampled schemes from all schemes (30 s sonication) 20

5 Selected under-sampled schemes from all schemes at reduced sonication lengths 21

6 Selected under-sampled schemes from all schemes for multiple slices 22

List of Figures

1 Gradient echo keyhole k-space example 5

2 k-space acquisition patterns 7

3 RTHawk user interface 8

4 Digital phantom and input ultrasound pulse 10

5 Process of under-sampling and temperature reconstruction 12

6 Axial slice of phantom along with time-temperature curve 15

7 Time-temperature curve : Bioheat Transfer Equation 15

8 Temperature measurement errors for low-frequency data 16

9 Temperature measurement errors: unsynchronized sequential acquisitions . . 18

10 Temperature measurement errors: synchronized sequential acquisitions (best case) 18

11 Temperature measurement errors: synchronized sequential acquisitions (worst case) 19

12 Temperature measurement errors: synchronized center-out acquisitions (best case) 19

13 Temperature measurement errors: synchronized center-in acquisitions (best case) 19

14 Temperature maps of selected under-sampled schemes 21

15 Time-temperature curve (1 slice) 23

16 Time-temperature curve (4 slices) 24

1 Introduction

1.1 Principles of MR-guided Focused Ultrasound

Magnetic Resonance-guided Focused Ultrasound (also known as MRgHIFU) is a hybrid technology that aims to offer non-invasive ablation of tumors and other soft tissues. The ultrasound energy is focused deep within the body, and the energy absorption by the target tissues causes a thermal effect that causes ablation. MRI offers accurate targeting due to its anatomical detail, real-time temperature monitoring by MR thermometry, and post procedural assessment owing to its rich image contrast.

1.2 Applications of HIFU

High Intensity Focused Ultrasound (HIFU) is used in a variety of medical applications, but with major focus in oncology. HIFU is currently under development for oncologic targets such as prostate, breast, liver, pancreas, bones and brain [1]. Some of these are in more clinically advanced stages than the others, however HIFU is being developed as a promising, non-invasive treatment method for tumors in different organs and body parts. Improvements in HIFU include research efforts that aim at better targeting, better temperature estimates, more advanced engineering of transducers and overcoming motion effects.

1.3 Magnetic Resonance Thermometry

A primary reason for choosing MR to monitor HIFU treatments over ultrasound is that it can provide accurate temperature estimates. When HIFU is being used for ablation, the goal is to achieve real-time temperature mapping to provide control over the treatment outcome [2]. Because these treatments are non-invasive, it is critical that clinicians be able to predict the heat deposition pattern, monitor the treatment in real-time and determine when a region of tissue has been treated to satisfaction [3]. A high spatiotemporal resolution is required to accurately measure the focal zone heating, because tissue temperatures in the focal zone can

rise as quickly as 3°C/s and the thermal dose doubles with every 1°C rise in temperature [4]. MR-thermometry is thus crucial in guiding HIFU treatments, and is mostly the given choice of monitoring treatments and is under constant research developments for improvements.

Given how quickly temperature rises, these temperature estimates need to be acquired at a quick frame rate. Typical thermometry protocols for closed-loop ablation of uterine fibroids can image up to six slices approximately every 3 s [5]. To explain simply, if we can only sample temperatures every 3 s, we might miss out on higher temperatures that may have occurred within those 3 s, which could lead to overheating and inaccurate thermal dose estimates. Hence, a need for faster temperature measurements is required, leading to a need for accelerated sequences.

A number of MR parameters show sensitivity to temperature, which leads to more than one way to use MR to measure temperature. Some of these parameters are proton density, T1 and T2 relaxation times, diffusion coefficient, magnetization transfer and proton resonance frequency (PRF) [1]. In all these methods, the most commonly used one is proton resonance frequency shift (PRF Shift) phase mapping thermometry.

1.4 Proton Resonance Frequency

The basis for MR thermometry is that hydrogen electrons shield the nucleus from the magnetic field which decreases the resonant frequency of the protons. Normal water molecules have hydrogen bonds between them which increase the resonant frequency of the protons by pulling electrons away from them. However, when the temperature rises, the bonds between these water molecules bend, stretch and break, which causes the resonant frequency of the protons to drop by an amount that is proportional to the increase in shielding of the protons by the electrons. This drop in resonant frequency is proportional to the increase in temperature, which is reflected in the phase images [1]. Briefly, PRF is used in gradient-echo sequences where phase images are obtained before and after heating. Phase differences

images are proportional to the change in temperature by the following equation:

$$\triangle T = \frac{(\phi - \phi_0)}{\gamma \alpha B_0 T E} \tag{1}$$

where $\triangle T$=change in temperature, ϕ_0=baseline image (phase image before heating), ϕ=phase image after heating, γ=gyromagnetic ratio, α=PRF change coefficient, B0= magnetic field strength and TE= echo time.

PRF phase shift mapping offers a number of advantages over other MR thermometry methods. Except for fatty tissue, α is independent of tissue type. Furthermore, it provides good linearity of signal with temperature over a large, relevant temperature range (-15°C-100°C). PRF has some drawbacks, primarily that it is sensitive to tissue motion and susceptibility changes and it does not work in fat. Despite these drawbacks, PRF is the most accepted way to measure temperature with MRI.

1.5 Pulse Sequences for MR Thermometry

A number of sequences have been tried to obtain fast temperature measurements in PRF based thermometry. Firstly, only gradient-echo sequences and not spin-echo sequences can be used for PRF based thermometry because the 180°pulse in spin-echo sequences rephases the temperature-dependent phase changes that occur due to heating. Currently, a gradient echo pulse sequence is most commonly used to this effect [6], however, for ideal echo times of T2*, long TE and TR settings are required, which can impose limits on acquisition speed [1, 6]. To overcome this problem, gradient-echo EPI sequences are used to speed up the acquisition, where many lines of k-space can be acquired within one TR, thus making optimal use of the long TR time. However, these come with their own drawbacks, the main ones being blurring and reduction in SNR. To improve SNR, an EPI-keyhole (EPIK) imaging technique was proposed (mainly for fMRI applications), where each acquisition consists of a central keyhole (acquiring the center of k-space densely) together with interleaved acquisition of

the outer k-space lines [7]. This method had advantages over single-shot EPI, the main one being improved spatial resolution, but the SNR stayed the same. Even though EPIK offers improved temporal resolution [7], it still faces the problem of artifacts that include distortion, blurring as all EPI sequences do. To overcome some of these issues, gradient echo keyhole sequences were proposed in this paper.

1.6 Pennes Bioheat Transfer Equation

Pennes Bioheat Transfer equation (PBTE or BHTE) [8], which describes the magnitude of exchange of heat transfer between tissue and blood, is widely used to solve temperature distribution for thermal therapy. The equation can be stated as follows:

$$\rho_t c_t \frac{\partial T}{\partial t} = \nabla.(k\nabla T) + w_b c_b (T - T_a) + < q > \tag{2}$$

where k=thermal conductivity [W/m°C], w_b=blood perfusion [kg/m^3s], c_b=specific heat of tissue [J/kg°C], T=tissue temperature [°C], T_a=arterial blood temperature [°C],$< q >$=power deposition [W/m^3]. In ablative procedures such as HIFU, the input energy increase the temperature at the target site. The BHTE is applied to model the process of energy deposition into the tissue and the resultant conduction/convection heat transport to tissue near the targeted site to predict temperature distribution.

2 Methods

2.1 Gradient Echo Keyhole and Trajectory Design

To combine the advantages of using a keyhole without EPI artifacts, and to increase acquisition speed while trying to maintain SNR, under-sampled gradient-echo keyhole trajectories for PRF thermometry were tested here. Gradient echo keyhole sequences have two characteristics: they acquire low frequency data more densely and high frequency data more sparsely,

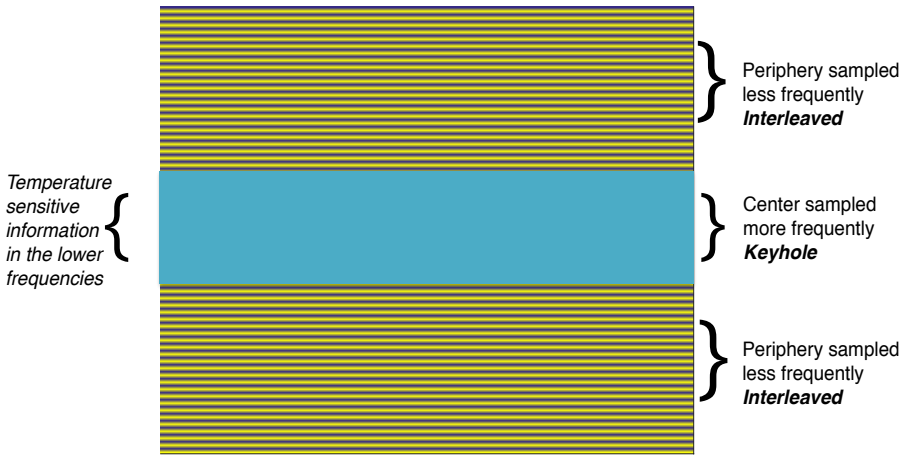

Figure 1: Gradient echo keyhole k-space example showing 2 interleaves with 32 keyhole lines. The purple lines are updated in odd frames, the yellow lines are updated in even frames and blue keyhole lines are updated in every frame.

and they eliminate distortion artifacts since each line of k-space is acquired in one TR. The temperature-sensitive information is assumed to be in the middle of k-space because the general shape of the temperature profile is dictated by the lower frequency information in k-space. Since the low frequency information lies in the middle of k-space, the temperature information should lie in the middle of k-space. Thus the middle of k-space is sampled in every frame whereas the outer-parts of k-space are not sampled as often. This results in an acceleration, which means temperature estimates can be obtained more frequently (more points along the time-temperature curve).

k-space data was under-sampled in various ways. The under-sampling was done in the phase encode direction and was a combination of two things: (1) Varying the keyhole size (2) Varying the number of interleaves. How this worked can be explained with an example as seen in figure 1. (2 interleaves with a keyhole size of 32). For phase encode lines running from 1-128, the purple (odd) lines are updated in every odd frame, the yellow (even) lines in even frames and the blue keyhole is updated in every frame (the lines are acquired in a top-to bottom fashion). The keyhole consists of 32 lines of central k-space where the low frequency data is contained. The alternating peripheral k-space lines are updated every other frame,

which here implies an interleave factor of 2. Thus, high frequency data is not as frequently acquired, based on the hypothesis that it contains more edge information and less temperature sensitive information. The combination of the two factors results in an acceleration rate. Examples of these can be seen in table 1. The first entry in table 1 is a fully acquired k-space, where all 128 phase encode lines are acquired, resulting in no acceleration.
To observe the effect of acquiring different parts of k-space at different times in the frame, k-space acquisition pattern was varied in two ways:

Sequential

k-space data was acquired in a sequential fashion first, which means that the lines were acquired in a top to bottom fashion (the phase encode direction is top-bottom).

Center-out

k-space data was also acquired in a center-out fashion, which means that the middle line was acquired first, and then followed by the line above it, and then back to the line below it. Thus, in each frame, the low frequency data was acquired first followed by the high frequency data. This acquisition pattern can be visualised in figure 2.

Table 1: Examples of under-sampled schemes and corresponding acceleration factors

Number of Interleaves	Keyhole Size	Acceleration Factor	Time taken per frame
1	128	1	3.66
2	32	1.66	2.33
4	24	2.66	1.37
7	9	4.92	0.74

2.2 RTHawk Implementation

RTHawk (HeartVista, Inc., Menlo Park, CA) allows real-time imaging (figure 3) and building of pulse sequences with customized interfaces. These trajectories were built into javascript

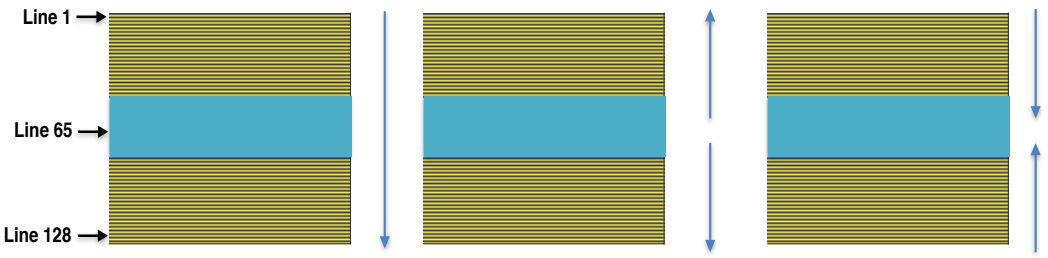

Figure 2: k-space acquisition patterns . Sequential acquisition(left): lines acquired in a serial order from top to bottom. Center-out acquisition(middle): low frequency lines acquired first, followed by outer, higher frequencies. Center-in acquisition(right): high frequency lines acquired first, followed by inner, lower frequencies.

files, and edited according to the number of k-space lines acquired per frame and the order in which they were to be acquired. A thermometry pipeline was built which allowed real-time data collection in both the axial and coronal views (axial view is along the ultrasound beam and coronal view is perpendicular to the ultrasound beam). The data was acquired in .dat files and then processed in MATLAB (R2016a, MathWorks, Natick, MA) for temperature reconstruction.

2.3 Phantom Data Acquisition

Data acquisition was carried out on a tissue-mimicking gel phantom. A 3T MRI (GE Healthcare, Waukesha, WI) scanner with an ExAblate 2100 (InSightec, Haifa, Israel) focused ultrasound system was used. The phantom was placed in a degassed water bath bucket, while ensuring that there were no bubbles between the phantom and the water, and the bucket and the table. Images of the phantom were obtained on the MR system (FA=30, TR=28.6 ms, TE=13.44 ms, BW=62.50 kHz, matrix size=256 x 128, FOV=28 cm, slice thickness=3 mm, resolution=1.12 mm x 2.25 mm) and then connected to the RTHawk system for real-time control. The HIFU sonications were performed with a rectangular phased-array transducer. The sonications were 30 s long, with an acoustic power of 3.35 W. Each view (coronal and axial) was acquired twice, so that they could be averaged out to eliminate experimental

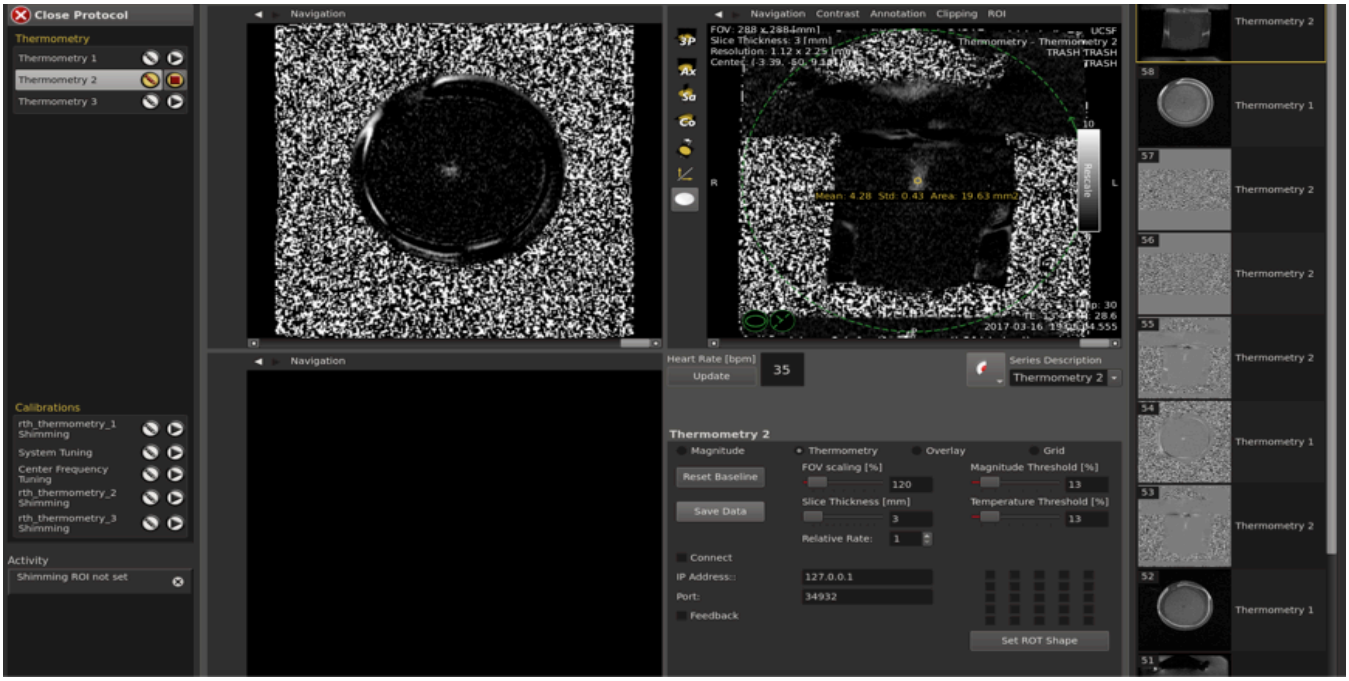

Figure 3: RTHawk user interface. The images are acquired in real-time. The coronal (left) and axial (right) views can be seen and run independently. RTHawk lets you reset the baseline, save the data and create an ROI around the hot-spot.

errors.

Retrospective Under-Sampling

Since only limited MR time was available for phantom data acquisition, only the fully-sampled k-space was acquired for sequential and center-out fashions. In order to test how different under-sampling schemes affect the temperature resolution, the fully-acquired data was retrospectively under-sampled. To achieve this, the baseline frame was first set by using a frame before heating started. This frame was used for all reconstructions, while only updating the middle low-frequency data (keyhole of varying sizes) in each new frame created while heating. These k-space matrices were then reconstructed using standard PRF thermometry, described in the section 1.4.

MATLAB Reconstruction

MATLAB was used for all post-processing and data analysis. The .dat files were imported into MATLAB, and the k-space matrix was built from the existing complex data in the raw dat file of each acquisition. MATLAB was used to retrospectively under-sample the fully-acquired k-space by zeroing out the data in different under-sampling schemes. PRF thermometry images were reconstructed from under-sampled data. No additional k-space filtering was used. The complex data in all frames was then subtracted from the baseline frame, and temperature was obtained using the PRF equation (equation 1).

This was done for various under-sampling schemes, and the temperature maps of the phantom were obtained. These were then used to create the time-temperature profiles in two ways: (1) temperature of the hottest spot in the center of the phantom over time (2) average temperature of a 5x5 pixel ROI around the hottest spot over time.

2.4 Mathematical Simulation Based on the Bioheat Transfer Equation

An entire simulation was built on MATLAB, which allowed the building of a 2-D digital phantom with specific acoustic properties, specify ultrasound input parameters, and then create time-temperature curves forward predicted by Pennes Bioheat Transfer Equation. This allowed to reduce dependancy on scan time for testing schemes, eliminate effects of experimental errors on predicting maximum temperature values, and to compare the different under-sampled schemes. The BHTE was used as a theoretical gold-standard, as it is used in many thermal modelling situations and reasonably approximates temperature elevation in tissues, taking the true physical and acoustic parameters of the tissue being considered [9, 10]. MATLAB was used to build a digital phantom (phantom built by Dr. William Grissom, Vanderbilt University, figure 4). This phantom had similar acoustic properties as

the actual phantom used. The BHTE was used to then construct a thermometry curve for a 30 s sonication. Assuming that thermal conductivity (k) is uniform throughout this digital phantom, equation 2 can be restated in its 2-D form as follows:

$$\rho_t c_t \frac{\partial T}{\partial t} = k(\frac{\partial^2 T}{\partial x^2} + \frac{\partial^2 T}{\partial y^2}) + w_b c_b (T - T_a) + < q > \tag{3}$$

In equation 3, x and y refer to the coordinates of the 2-D phantom (seen in figure 4). For the purpose of this simulation, the energy deposition is assumed uniform in z, and the 2-D phantom being considered is thus a cross-section of the plane at the focus of the ultrasound pulse. The following parameters were chosen for the variables in equation 3: ρ= 1060 kg/m^3, C_t, C_b = 4186 J/kg/°C, k = 1 W/m/°C, W = 0 $kg/m^3/s$, Q = 3.5 W/m^3.

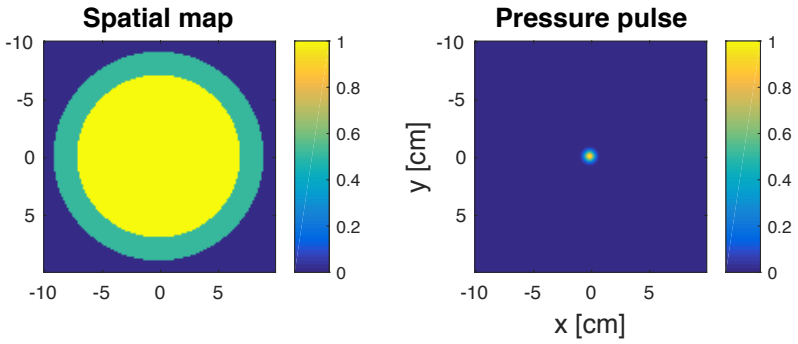

Figure 4: Digital phantom and input ultrasound pulse. The digital phantom has the highest magnitude intensities in the inner circle and the intensity is zero outside the phantom. The pressure pulse focuses its energy in the middle pixel, followed by a distribution of energy that fades off gradually in a radial direction.

Additionally, sonications were 30 s long, B_0= 3 T, TR=28.5 ms and TE=13.4 ms. All the values were chosen to best imitate the experimental results and actual phantom properties. k-space data was then created (described in the next section). This k-space matrix was now under-sampled in various desired forms and then reconstructed to create thermometry images to visualize the hot spot. The under-sampling was done in the same way as described in section 2.1. However, since no MR time was required, a lot of schemes were developed. Under-sampling was done in three ways: (1) Using only the middle low-frequency k-space

lines (2) Using only lines that are interleaved throughout k-space (3) Using a combination of low frequency lines densely sampled and high frequency sparsely sampled (described in section 2.1). Also, the pattern of k-space acquisition was varied. Data was acquired in three fashions: sequentially, center-out and center-in. This was done in order to observe the effect of the temperature sensitive data being acquired at different parts of the frame: in the middle, in the beginning and towards the end. For all under-sampled schemes, two metrics were measured in order to measure performance of the curves: difference in maximum temperature obtained by under-sampled k-space and obtained by BHTE [%] and difference in the average temperature of a 5x5 ROI around the hottest spot obtained by under-sampled k-space and obtained by the BHTE [%].

2.5 Under-sampling and Reconstruction Process

The BHTE was used to forward predict the temperature with the ultrasound input on the digital phantom. After obtaining temperature values for each pixel in each frame, the entire frame was converted to a phase map using the following equation: (obtained by rearranging equation 1)

$$\phi = (T_n) \times 0.01 \times 10^{-6} \times B0 \times TE \times \gamma \tag{4}$$

These phase maps were then combined with the magnitude data to create the complex data. The complex data was Fourier transformed into the k-space which was then under-sampled. After obtaining the desired under-sampled k-space, an inverse Fourier transform was performed to get the new complex data, which was converted to the temperature map using the following equation:

$$T_{new} = \frac{\phi}{(0.01 \times 10^{-6} \times gamma \times B0 \times TE)} \tag{5}$$

This whole process can be visualized in figure 5.

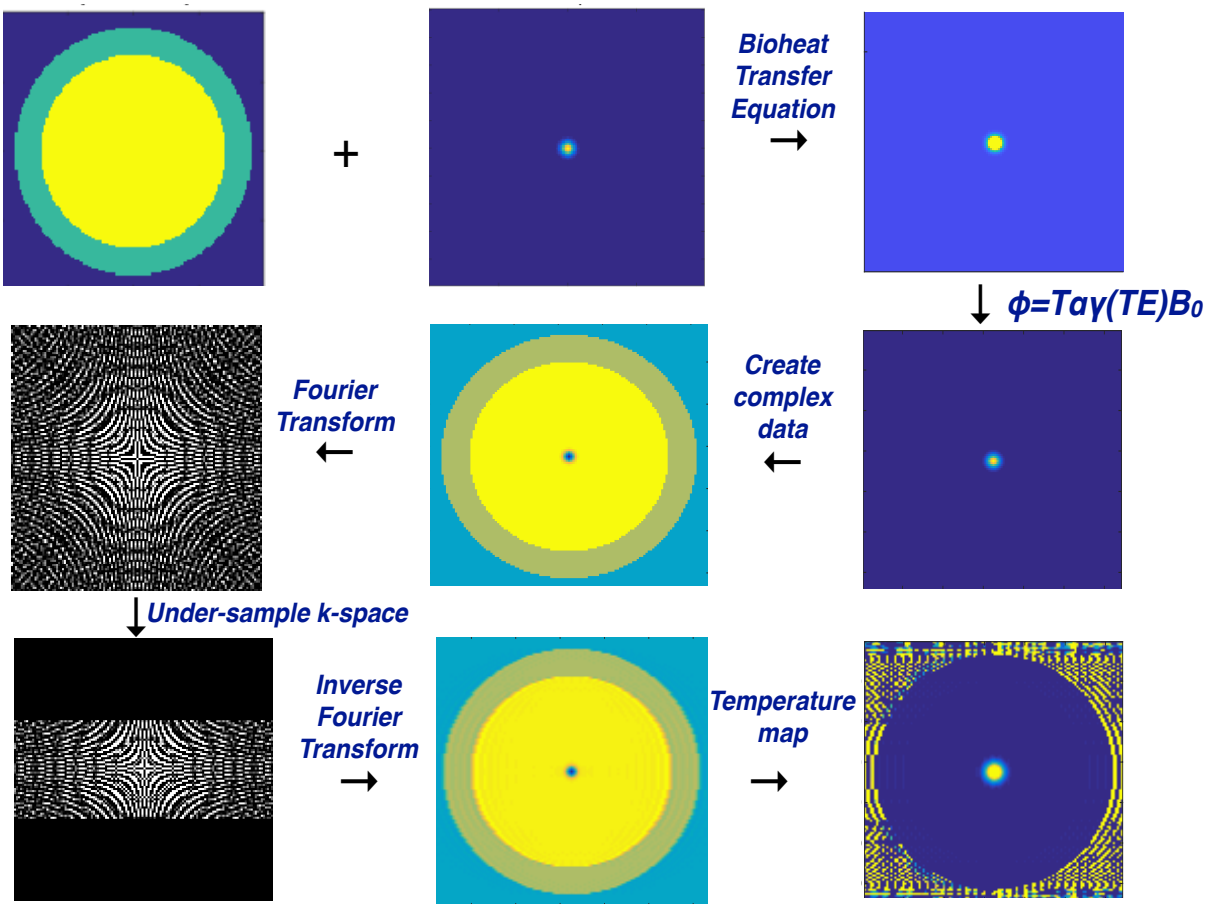

Figure 5: Process of under-sampling and temperature reconstruction. Top left to bottom right: the digital phantom and input pulse result in a temperature map and its corresponding phase data, which is combined with magnitude data to create the complex data. This is fourier transformed to the k-space, which is then under-sampled. The process is reversed to obtain a new temperature map created from the under-sampled k-space.

2.6 Synchronization

Another thing that was looked at to address the concern that the data acquisition was not synchronized to the sonication. Since under-sampled schemes imply that different lines of k-space are being acquired, there was no consistency between the different schemes regarding which part of k-space was being acquired when the maximum temperature was reached

(when the sonication ended). Based on the assumption that the middle of k-space has the most temperature sensitive information, these chosen under-sampled acquisitions were then synchronized to the sonication. To include the best and worst case scenario, the acquisition was shifted in order for the sonication duration to coincide with two points in k-space: in the center of k-space and at the end of k-space. The best case was hypothesized to better predict the maximum temperature in all under-sampled schemes, since the center of k-space is assumed to contain the temperature sensitive information within the low frequencies.

2.7 Reducing Sonication Time

The under-sampled schemes were first tested in 30 s long sonications. However, for many focused ultrasound applications (like hyperthermia) the sonications are as short as 3 s. To test the feasibility of the under-sampled schemes in different applications in focused ultrasound, these schemes were also tested in reduced sonications lengths of 15 s and 3 s.

2.8 Faster Frame Rate for Multiple Slices

Typically, during focused ultrasound treatments, an entire volume is monitored for change in temperature. To this effect, the temperature values for different slices are obtained at increased speeds. Most commonly, this is done with EPI sequences. However as discussed in section 1.5, EPI sequences come with their own drawbacks. Thus, to test their feasibility in observing temperatures in multiple slices, thermometry curves were built for the selected schemes for multiple slices. An example of how this was done: assume that one temperature estimate takes 1.9 s for a selected under-sampled scheme. If there are 4 slices that are acquired consecutively and if time starts at 0, then in 1.9 s the temperature for the first slice will be obtained. From 1.9 s to 3.8 s, the k-space of the second slice will be acquired and the second slice temperature will be obtained at 3.8 s. This will occur until 7.6 s (=1.9 s x 4), which is when all four slices will have had one temperature estimate each. At 7.6 s, the k-space of the first slice will be updated and the second temperature for slice 1 will be obtained

at 7.6 s+1.9 s = 9.5 s. Therefore, since the gap between any two temperature estimates in one slice increases when the number of slices increases, faster frame rates with accurate temperature measurements are required to obtain temperature measurements in multiple slices. For this simulation, the temperature of only one slice was estimated assuming that there are other slices being acquired, i.e, the temperature estimates for one slice were less frequent since other slices were also being acquired.

3 Results

3.1 Experimental Data

The sequentially acquired k-space resultant time-temperature profiles were reconstructed with varying keyhole sizes of 32, 64, 100, 126 with a 30 s sonication. Figure 6 shows an example thermometry image of the slice along with its time-temperature profile of the hottest pixel in figure 6. In figure 6, the difference in maximum temperature measured by the fully-sampled k-space and that by the middle 32 lines is 12.51%. As seen, the keyhole sizes 64, 100 and 126 are doing as well as the fully acquired k-space.

Similarly, the same experiment was carried out on coronal views for both sequential and center-out acquisitions. In all the results, only the 32 under-sampled trajectory showed differences, and the rest had no differences from the fully-sampled curve. These results are summarized in table 2 below:

Table 2: Results of phantom experiments

Experiment number	Acquisition Pattern	View	Difference between maximum temperature predicted by 128 lines and 32 lines of k-space
1	Sequential	Axial	12.51%
2	Sequential	Coronal	8.97%
3	Center-out	Axial	15.54%
4	Center-out	Coronal	14.46%

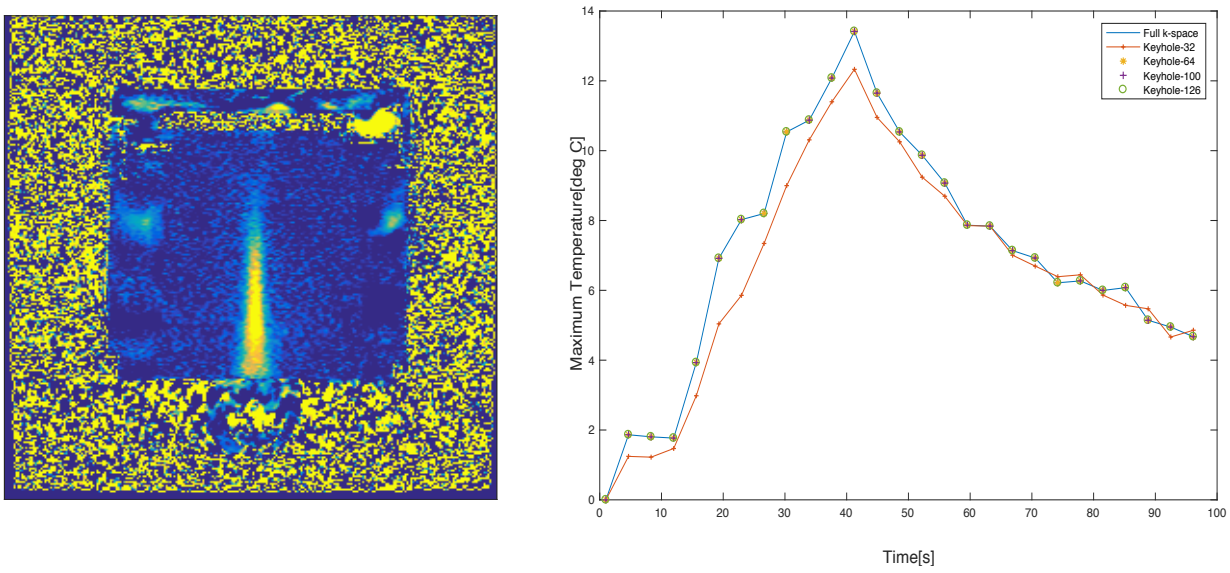

Figure 6: Axial slice of phantom along with the time-temperature curve for the hottest pixel in the phantom. The focusing of the ultrasound pulse can be visualised here, and the curve represents the temperature of the hottest point in this slice. Compared to the fully-acquired k-space, refreshing only the middle 32 lines of k-space underestimates the temperature, but using 64, 100,126 lines do just as well as using all 128 lines.

3.2 Mathematical Model

The time-temperature curve for the maximum temperature predicted by the BHTE in the phantom was obtained and can be seen in figure 7. The peak temperature reached is 21.9°C at 30 s. The length of the simulation is 150 s.

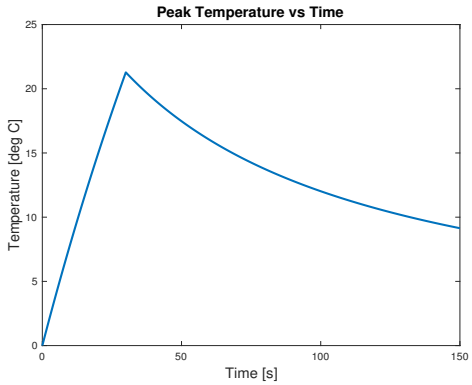

Figure 7: Time-Temperature curve predicted by Bioheat Transfer Equation for the digital phantom. This curve shows the temperature of the hottest pixel in the digital phantom obtained with a 30 s sonication over a 150 s long simulation.

3.2.1 Low Frequency Data Only

For the low frequency data only, the results can be visualized in figure 8. In figure 8, the difference in maximum temperature error reduces drastically after at least 39 lines have been acquired, where the error is 10.1%. In figure 8 these errors start to reduce for all lines after a threshold of 60 lines until which synchronization seems to have no effect. Table 3 shows the results of using 39, 42, 70, 75 lines of low-frequency data. These will be used for further analysis.

Table 3: Selected under-sampled schemes from low-frequency data only

Number of low-frequency lines	Factor increase in frame-rate compared to fully acquired k-space	Sychronized to middle of k-space?	Difference between maximum temperature predicted by BHTE and under-sampled k-space
39	3.28	No	10.10%
42	3.04	No	8.40%
70	1.82	No	0.91%
70	1.82	Yes	0.50%
75	1.70	No	0.50%
75	1.70	Yes	0.03%

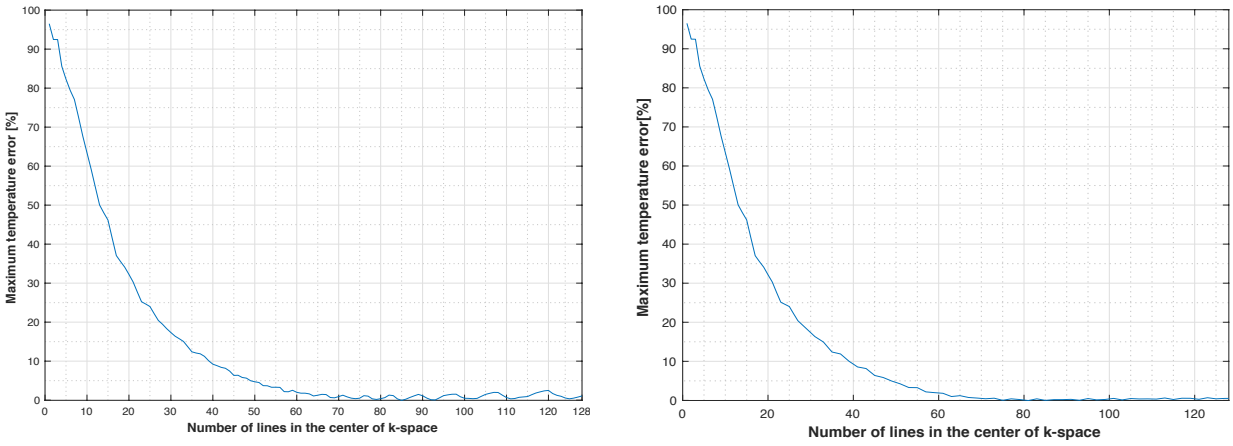

Figure 8: Temperature measurement errors for low-frequency data only. The figure on the left shows the errors when no synchronization has been performed, waves can be seen after 65 lines have been acquired. These errors flatten out when the sonication is synchronized to end at the center of k-space, which can be seen in the figure on the right.

3.2.2 Combination of High Frequency Data (Interleaved) and Low Frequency (keyhole) Data

Interleaves were varied from 2 to 7 and keyhole size was varied from 1 to 128. The difference in maximum temperature predicted by the BHTE and that predicted by the under-sampled scheme was calculated and plotted for all the under-sampled schemes for a 30 s sonication. These plots were generated for all acquisition patterns, but a selection of these are shown and discussed in this paper. The plots on the left are visualised in 3-D, whereas those on the right are in 2-D (figures 9 to 13).

Sequential Acquisition

Figure 9 shows the plot for the sequential acquisitions. The errors increase and reduce in waves as the number of lines acquired vary as the sonication ends in a different line of k-space for each scheme. To overcome this issue, the same schemes were synchronized for the sonication to end in the middle of k-space. These results can be visualized in figure 10, where the errors have significantly reduced. To further confirm the hypothesis that synchronizing to the middle of k-space gives more accurate estimates, the 3-D plot in figure 11 shows the same estimates for sequential acquisitions, but here the sonication ends at the end of k-space.

Center-out Acquisition

Figure 12 shows the plots for the center-out acquisitions. These results have been synchronized for the sonication to end in the middle of k-space. It can be seen that these results are not as good as the sequential acquisitions.

Center-in Acquisition

Figure 13 shows that center-in was found to have the least accurate temperature measurements compared to center-out and sequential acquisitions. Even in the best case, the results

were not as good. These are seen in figure 13, where the lowest possible error is 1% as compared to 0.1% in sequential (see figure 10).

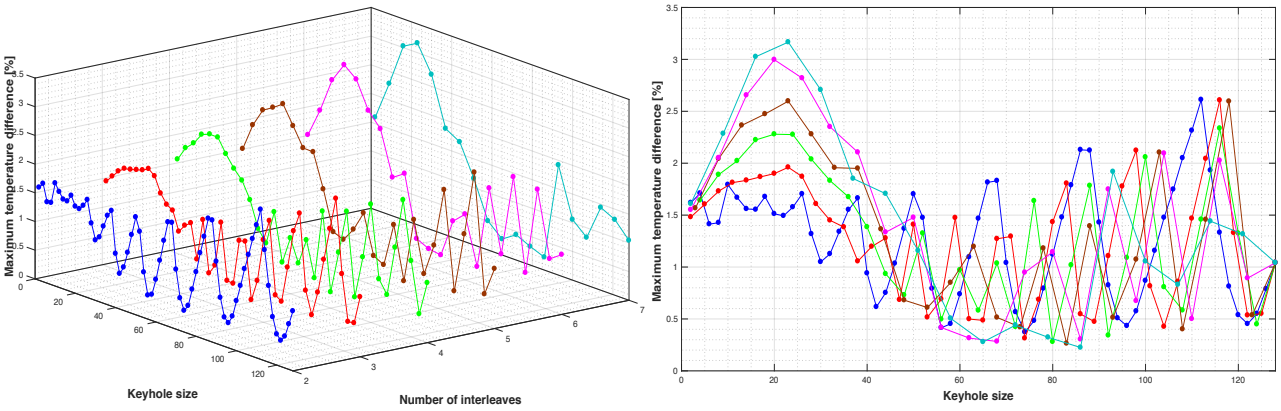

Figure 9: Temperature measurement errors: unsynchronized sequential acquisitions

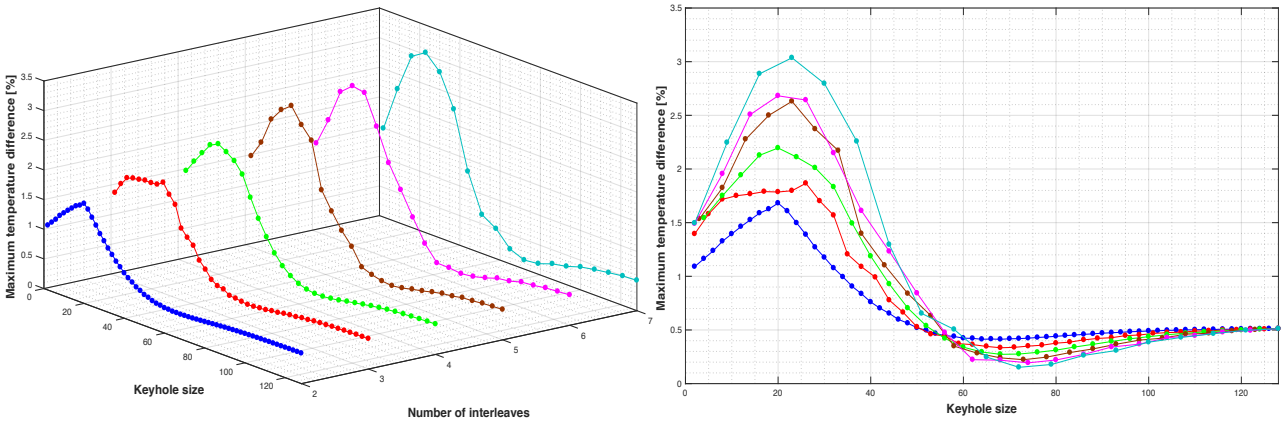

Figure 10: Temperature measurement errors: synchronized sequential acquisitions (best case)

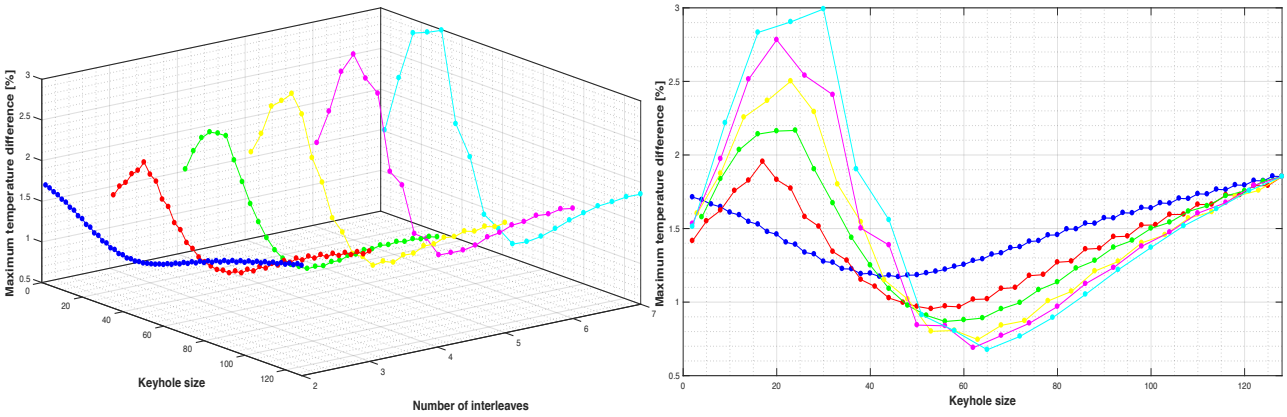

Figure 11: Temperature measurement errors: synchronized sequential acquisitions (worst case)

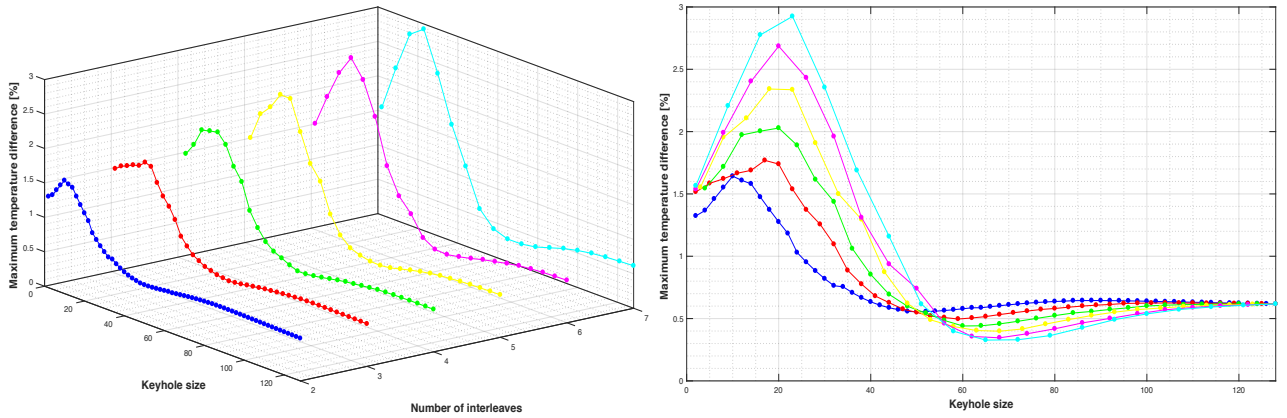

Figure 12: Temperature measurement errors: synchronized center-out acquisitions (best case)

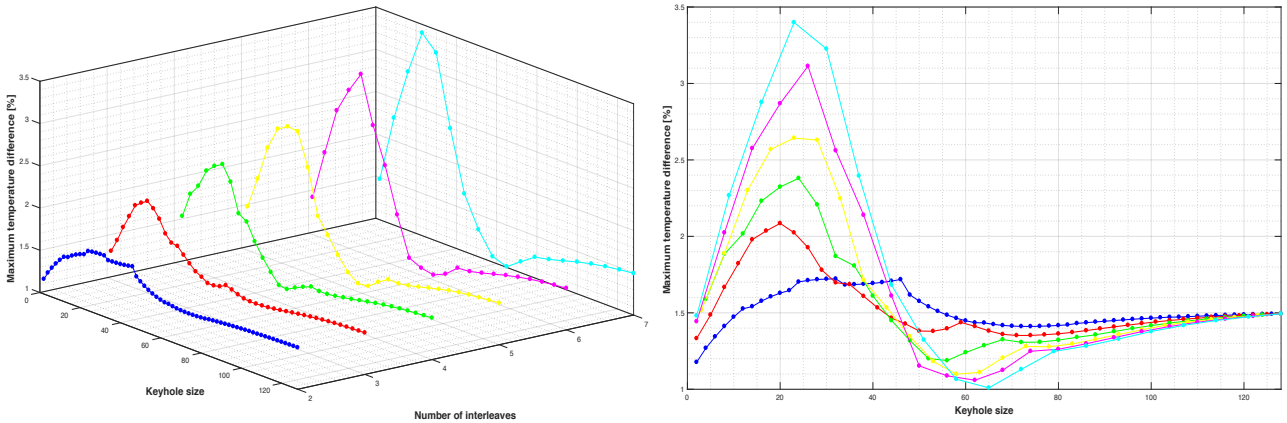

Figure 13: Temperature measurement errors: synchronized center-in acquisitions (best case)

Table 4 summarizes some of the under-sampled schemes picked up from these plots that have a frame rate increase factor of 1.6 or more. In figure 14, the evolution of the hot spot over time is visualised for two promising schemes, as compared to the BHTE hot spot. This figure visualises how the hot spot changes over time, it is small before the maximum temperature is reached, the brightest and sharpest at the hottest frame, and starts to dissipate heat as the temperature cools off after the ultrasound is switched off (Note: shorthands have been used to discuss particular schemes; ex: 3-32 would refer to 3 interleaves with a keyhole size of 32).

Table 4: Selected under-sampled schemes from all schemes (30 s sonication)

Under-sampled scheme	Acquisition pattern	Factor increase in frame-rate compared to fully acquired k-space	Sychronized to middle of k-space?	Difference between maximum temperature predicted by BHTE and under-sampled k-space
1-128	Sequential	1.0	No	1.07%
1-70	Sequential	1.6	No	0.91%
1-70	Sequential	1.6	Yes	0.50%
5-63	Sequential	1.68	Yes	0.28%
5-63	Center-in	1.68	Yes	1.11%
5-63	Center-out	1.68	Yes	0.40%
7-58	Sequential	1.88	Yes	0.50%
7-58	Center-in	1.88	Yes	1.06%
7-58	Center-out	1.88	Yes	0.39%

3.2.3 Reducing Sonication Time

Given that most of the selected schemes except center-in were doing well at 30 s, the effects of reducing sonication time were observed for the synchronized schemes to evaluate how robust they are to shorter sonications. These results are summarized in table 5.

Table 5: Selected under-sampled schemes from all schemes at reduced sonication lengths

Under-sampled scheme	Acquisition pattern	Difference between maximum temperature predicted by BHTE and under-sampled k-space at 30 s	Difference between maximum temperature predicted by BHTE and under-sampled k-space at 15 s	Difference between maximum temperature predicted by BHTE and under-sampled k-space at 3 s
1-70	Sequential	0.50%	0.80%	1.39%
5-63	Sequential	0.28%	0.79%	6.46%
5-63	Center-in	1.11%	1.42%	5.79%
5-63	Center-out	0.40%	0.49%	4.87%
7-58	Sequential	0.50%	1.18%	7.75%
7-58	Center-in	1.06%	1.43%	9.09%
7-58	Center-out	0.39%	0.66%	8.43%

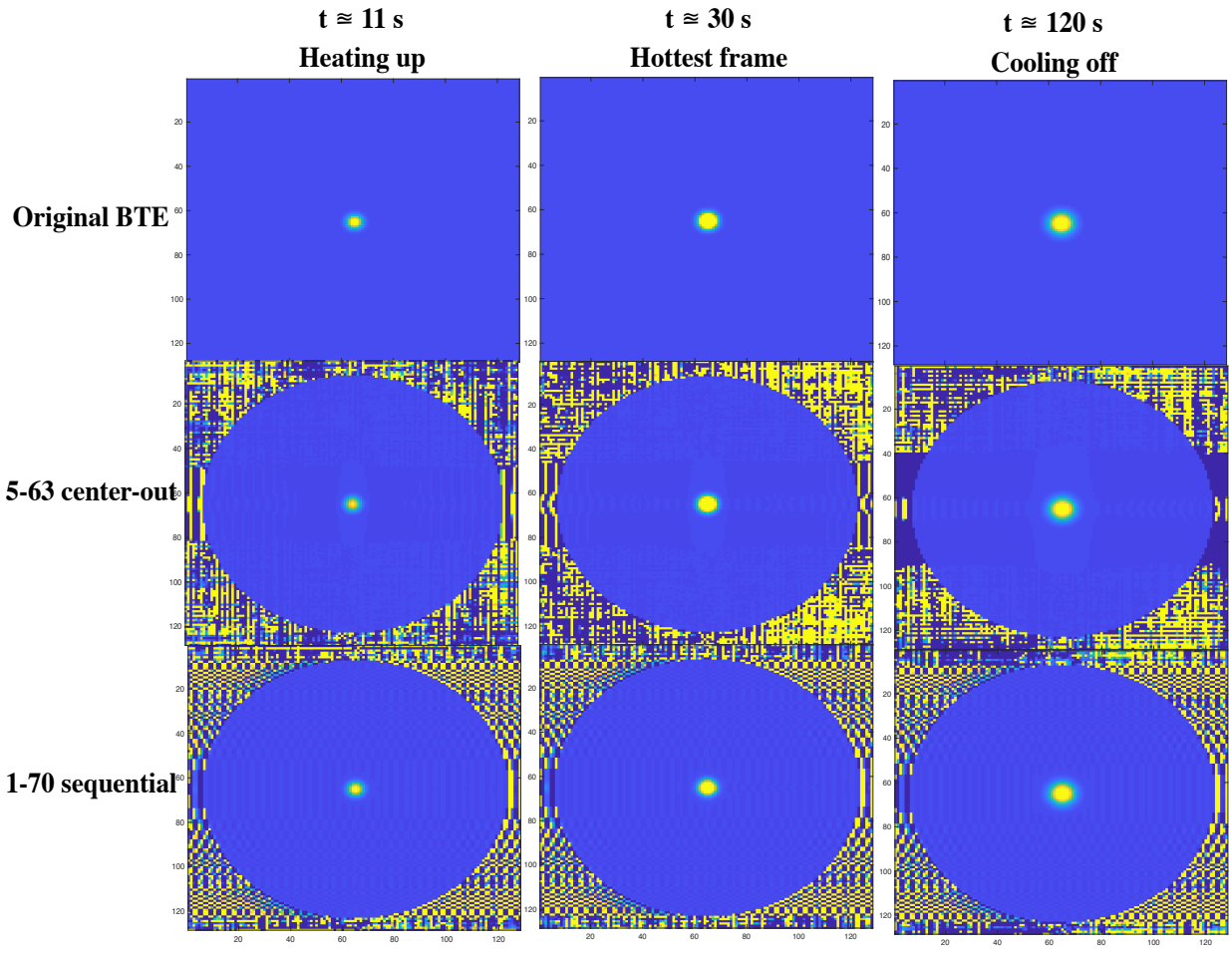

Figure 14: Temperature maps of selected schemes over time for a 30 s sonication, compared to the BHTE temperature maps.

3.2.4 Selected Schemes for Multiple Slices

The effect of adding other slices was observed on the under-sampled schemes. Table 6 summarizes the effect of increasing the number of slices on the maximum temperature error in any one slice. All sonications were held at 30 s. Number of slices were varied at 1, 4 and 8. As expected, errors increase as more slices are added. The time-temperature curve for the hottest spot in the first slice for some of these selected schemes when 1 slice is being monitored and when 4 slices are being monitored are shown in figure 15 and 16, respectively.

Table 6: Selected under-sampled schemes from all schemes for multiple slices

Under-sampled scheme	Acquisition pattern	Difference between maximum temperature predicted by BHTE and under-sampled k-space (1 slice)	Difference between maximum temperature predicted by BHTE and under-sampled k-space (4 slices)	Difference between maximum temperature predicted by BHTE and under-sampled k-space (8 slices)
1-70	Sequential	0.50%	1.88%	1.88%
5-63	Sequential	0.28%	4.21%	12.27%
5-63	Center-in	1.11%	5.66%	7.66%
5-63	Center-out	0.40%	4.96%	10.76%
7-58	Sequential	0.50%	5.49%	5.49%
7-58	Center-in	1.06%	4.87%	7.17%
7-58	Center-out	0.39%	4.29%	9.55%

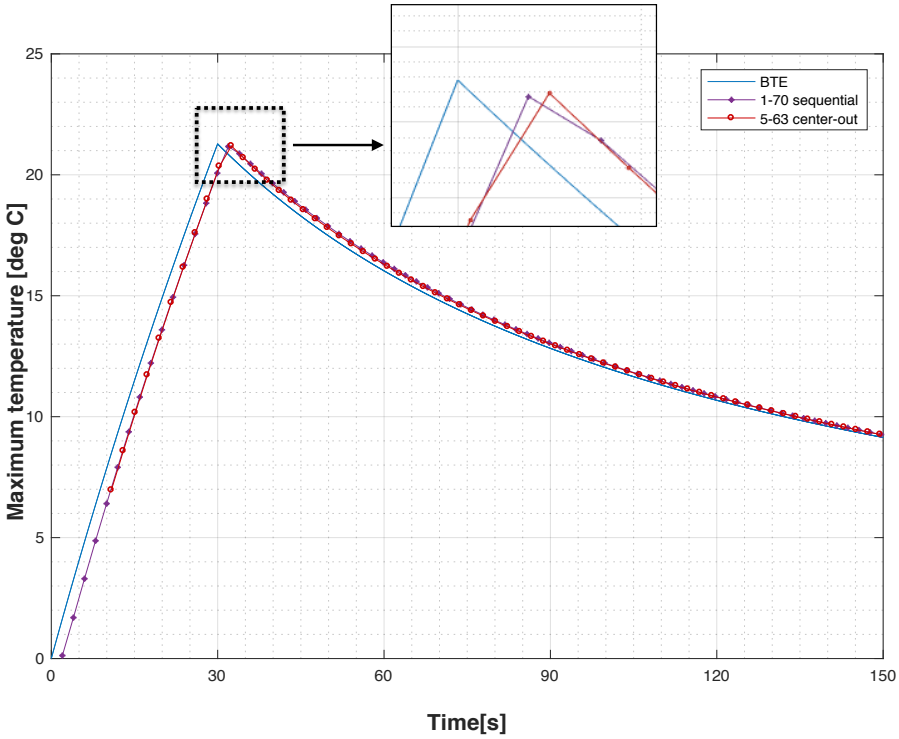

Figure 15: Time temperature curves for monitoring temperature in 1 slice only with different under-sampled schemes. In the purple curve, an increased frame rate of 1.8x of the 1-70 scheme compared to 1.68x for the 5-63 scheme can be visualised. Additionally, since 5-63 has 5 interleaves, the first temperature estimate is only obtained once 5 frames have been acquired. In the zoomed in peaks of the curve, not much difference in temperature is seen between the two under-sampled schemes and the BHTE.

4 Discussion

4.1 Experimental Data

In the experimental data, it can be seen that acquiring only 64 lines of k-space also gives almost 100% temperature accuracy compared to a fully-sampled k-space, according to figure 6. This result implies that in experiment, instead of refreshing all 128 lines per frame, refreshing even just the middle 64 lines can double the frame rate and still have the same results as using all 128 lines. Thus, acquisition speed in current gradient-echo experiments

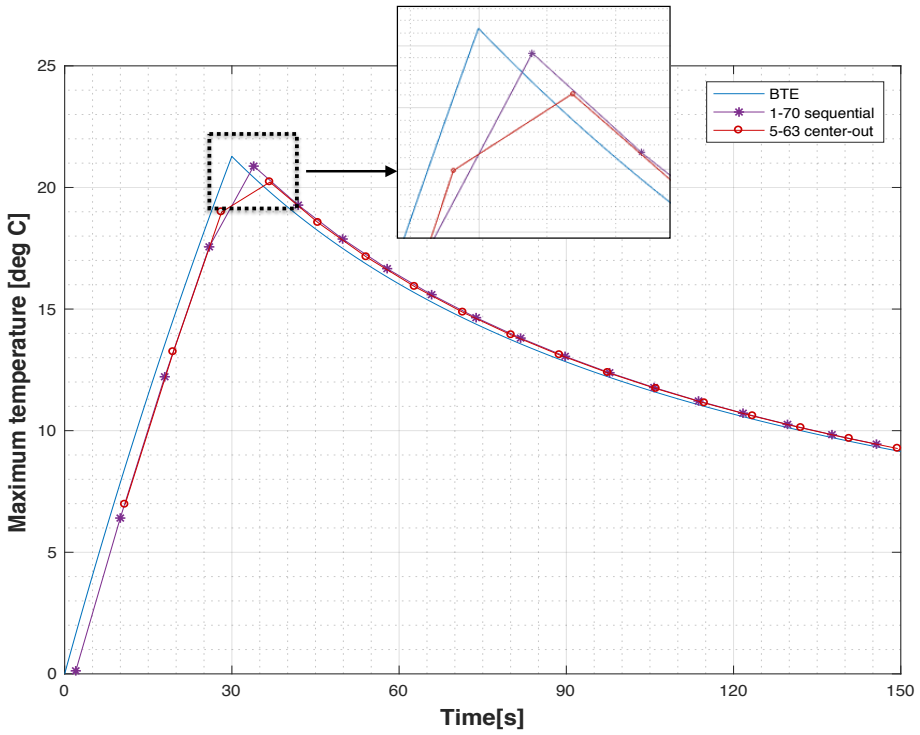

Figure 16: Time temperature curves for monitoring temperature in 1 slice when there are 4 slices present with different under-sampled schemes. In the purple curve, an increased frame rate of 1.8x of the 1-70 scheme compared to 1.68x for the 5-63 scheme can be visualised. Additionally, since 5-63 has 5 interleaves, the first temperature estimate is only obtained once 5 frames have been acquired. In the zoomed in peaks of the curve, there is a difference in temperature is seen between the two under-sampled schemes and the BHTE. The 1-70 scheme is closer to the maximum temperature estimated by the BHTE as compared to 5-63.

can be improved. Another observation is that the sequential acquisitions are doing better than the center-out acquisitions according to table 2. This is in agreement with the simulated data from the mathematical model too. Center-in acquisitions could not be tested in the initial phantom experiment due to lack of MR time.

Even though the experimental data was retrospectively under-sampled, it was not sufficient to test all the under-sampling schemes to decide which ones would work well. There were a number of reasons for this: (1) The experimental data was still imperfect, even after averaging out. The experiment was run manually and there was experimental noise and other imperfections, which makes comparison of the under-sampled schemes difficult. (2)

The start of the data acquisition had not been synchronized with the start of the sonication, since they were both done manually. This means that even a slight delay between the start of the acquisition and the sonication could have impacted the measured hottest point, since a delay would imply that a different line of k-space was being acquired. Additionally, this experiment was not an ideal way to test synchronization, since there was no way to automate a calculated delay between the start of the sonication and the acquisition. (3) Even with retrospective under-sampling, the true increased frame rate could not be reflected in the time-temperature curves. (4) The gold standard was considered to be the fully acquired k-space, which itself was not perfect data and thus made it hard to make comparisons with under-sampled k-spaces. Additionally, as mentioned in section 1.3, extracting temperature every 128 lines of k-space (=3.64 s with a 28.5 ms TR) might not be quick enough for accurate temperature estimates.

4.2 Low-frequency Data Only

In figure 8, the fact that the errors reduce drastically around 39 lines (10.10% error), shows that a lot of the temperature information is contained in the middle 39 lines. At 70 lines, this error reduces to 0.91%. Compared to 3.64 s for acquiring all 128 lines, acquiring 70 lines only takes 1.99 s and provides good estimates compared to the BHTE. Unexpectedly, even after acquiring 70 lines, the errors increase and reduce in waves even as the number of lines increases. This confirms the hypothesis that the error is not only dependent on how many lines are acquired, but also which line is being acquired when the sonication ends. Between the two graphs in figure 8, the errors only seem to flatten out after around 60 lines have been acquired. This shows that synchronization only starts to have an effect after a certain number of lines have been acquired. These results are especially important when these schemes will be used in reduced sonication lengths. For example, table 5 shows that reducing the sonication length for sequentially acquired middle 70 lines of k-space doesn't have a great impact on temperature prediction accuracy and would therefore make a good choice for an

under-sampled scheme when reducing sonication time. When monitoring multiple slices, according to table 6 and figure 16, 1-70 is a good choice. For example, in figure 15, 1-70 sequential offers no great benefit over using 5-63 center-out, however, its benefit is visible when the number of slices is increased to 4 in figure 16. However, it does not perform as well as 5-63 center-out at 30 s and 15 s, and therefore should be used for multiple slice monitoring at reduced sonication times. Additionally, in figure 14, the temperature maps for 1-70 sequential show that while the hot spot remains unaffected over time compared to the BHTE temperature maps, there are many more artifacts in this scheme due to the lack of outer k-space lines. However, this simulation was only concerned with the maximum temperature in the hottest spot, and this temperature was predicted to a 0.50% accuracy. If temperature was to be recorded outside the hot spot, this scheme would not perform as well as 5-63 center-out.

4.3 Combination of High Frequency Data (Interleaved) and Low Frequency Data

For all acquisitions, in figures 10, 11, 12 and 13 it can be seen that for smaller keyhole sizes (between 0-40), increasing the number of interleaves increases the error in temperature prediction. This pattern is reversed in moderate keyhole sizes (between 60-80), where increasing the number of interleaves reduces temperature prediction error. It could be further inferred that if more than 7 interleaves had been simulated, these errors would reduce even further. However, this reduction would not be much since the error reduction reduces as the number of interleaves increases. For example, this means that the difference in error between using 19 interleaves and 17 interleaves would be almost indiscernible. Due to this reason and computational limitations, this simulation only ran up to 7 interleaves. At very large keyhole sizes (100-128), the number of interleaves don't seem to matter, which is expected since barely any part of the k-space is left outside of large keyholes to be interleaved.

Overall, center-in performed the worst in all the acquisition patterns. This could be because

the temperature sensitive information is acquired towards the end of the frame, which also means that for the synchronized data the sonication ends at the end of the frame. However, acquiring the temperature sensitive information (which is in the center of k-space) in the beginning of the frame in the center-out acquisitions did not perform the best, which implies that the synchronizing the middle of k-space with the middle of the frame as sequential does could be the best way to measure temperature in focused ultrasound applications.

While selecting actual under-sampling patterns from keyhole data, 5-63 center-out is a feasible scheme to select. Of all the schemes, its errors remain under 5% at shorter sonication lengths of 3 s and when monitoring multiple slices (4 slices). As per frame rate, it acquires 1.68x more frames and has a smaller error in predicting maximum temperature when compared to acquiring all 128 lines (see table 4). When looking at its temperature maps in figure 14, 5-63 center-out has a hot spot that looks like the one predicted by the BHTE, and has fewer artifacts as compared to 1-70 sequential.

A very important observation that was made was that synchronizing the data acquisition to the sonication overall improves temperature estimates. This could not be implemented in the phantom experiment conducted prior to building the simulation, but now that it has been shown to work well, it could be implemented in future experiments. RTHawk uses a custom built thermometry pipeline that allows the order of k-space lines and which k-space lines are to be acquired. The pipeline could be modified to introduce a delay based on the number of lines acquired in any under-sampled scheme in order for the sonication end to coincide with the middle of k-space. These modifications can be introduced in the javascript build files in the the pipeline. A way to control the sonications from the RTHawk platform will have to be built into the pipeline for this controlled acquisition to be executed. Once achieved, much better temperature acquisitions, with a higher frame rate can be achieved compared to using all 128 lines of k-space in each frame.

4.4 Limitations of Simulated Model

While the limitations of the experimental data have already been discussed, the simulated model also had its own shortcomings. While multiple slices were briefly looked at, this simulation was entirely in 2-D. The slice numbers were varied discretely, and some of the errors could have been simply coincidental based on the acquisition pattern and number of slices. This means that, even though 1-70 sequential was robust to increasing the number of slices all the way up to 8, this would maybe not be the case if one more slice was added or one slice was removed. As stated in section 2.4, this 2-D phantom was the slice of the phantom at the focus of the pulse. The temperature-time curves for this were plotted, however, the ultrasound distribution in the other slices that are not the focus would be different, resulting in a different temperature distribution. This model also assumes no motion, which is an occurrence in all focused ultrasound applications due to breathing and intra-scan motion. The results presented here assume a constant value for k, c_b and sets w_b=0. In reality, these values can be different and have impact on the results. Lastly, one of the biggest drawbacks is that the model only assumes a single type of tissue, where the tissue density is specified by ρ. In actual treatments, the ultrasound inevitably comes across more than one tissue type in its path.

4.5 Future Directions

While the sonication lengths were varied in discrete lengths, the sonication lengths in between these discrete lengths were not simulated. These could have been explored especially if certain experiments require the sonication length to be continuously updated over a period of time in order to achieve controlled heating. In the code for the existing model, this could be implemented and the effects of various sonication lengths on temperature accuracy for different schemes could be looked at. As stated in the limitations, this model is 2-D only. If extended to a 3-D situation, in future simulations, the ultrasound beam can be modelled to a 3-D phantom resulting in a 4-D distribution of heat over x,y,z and time, which would

give better estimates for volumetric thermometry. This combined with different sonication lengths could help predict an entire treatment plan, especially if density values for other tissue types can be included by adding them to appropriate locations within the 3-D digital phantom. COMSOL Multiphysics (Burlington, MA, USA) could be used to build the 3-D phantom and the existing code could be used to call the functions for the model in COMSOL [11].

5 Conclusion

While this simulation had its limitations, a few conclusions can be arrived at with this data. Firstly, synchronizing the ultrasound pulse to the data acquisition has an impact on temperature measurements and should be implemented in future studies and experiments. Secondly, different under-sampled schemes perform differently based on the sonication lengths, and performance overall reduces when sonication lengths are shorter. For shorter sonications, using just the low frequency data does a more accurate job, and is easier to implement. Similarly, for monitoring temperature in more than one slice, using just the middle 70 lines sequentially provides good estimates. The opposite is true for longer sonications and single slice, where 5 interleaves with a 63 keyhole size acquired center-out performs better. A dynamic code that could implement changing acquisition patterns based on sonication lengths and number of slices being monitored would significantly improve temperature acquisitions. This could be implemented in RTHawk, where the feedback control not only changes the input power but also changes the kind of k-space acquisition. A validation study is important to confirm these results by comparing temperature estimates obtained by under-sampled schemes to the Bioheat Transfer Equation forward predicted temperatures. The validation could be performed in just a simple soft-tissue mimicking phantom as was used in the experiment and further studies could be explored in different kinds of tissue.

References

[1] Viola Rieke and Kim Butts Pauly. MR thermometry. *Journal of magnetic resonance imaging*, 27(2):376–390, 2008.

[2] Yu-Feng Zhou. High intensity focused ultrasound in clinical tumor ablation. *World journal of clinical oncology*, 2(1):8, 2011.

[3] Nick Todd, Urvi Vyas, Josh De Bever, Allison Payne, and Dennis L Parker. The effects of spatial sampling choices on MR temperature measurements. *Magnetic resonance in medicine*, 65(2):515–521, 2011.

[4] Nick Todd, Allison Payne, and Dennis L Parker. Model predictive filtering for improved temporal resolution in MRI temperature imaging. *Magnetic resonance in medicine*, 63(5):1269–1279, 2010.

[5] Pooja Gaur and William A Grissom. Accelerated MRI thermometry by direct estimation of temperature from undersampled k-space data. *Magnetic resonance in medicine*, 73(5):1914–1925, 2015.

[6] Jing Yuan, Chang-Sheng Mei, Lawrence P Panych, Nathan J McDannold, and Bruno Madore. Towards fast and accurate temperature mapping with proton resonance frequency-based MR thermometry. *Quantitative imaging in medicine and surgery*, 2(1):21, 2012.

[7] Maxim Zaitsev, K Zilles, and NJ Shah. Shared k-space echo planar imaging with keyhole. *Magnetic resonance in medicine*, 45(1):109–117, 2001.

[8] Harry H Pennes. Analysis of tissue and arterial blood temperatures in the resting human forearm. *Journal of applied physiology*, 1(2):93–122, 1948.

[9] Matthew S Adams, Serena J Scott, Vasant A Salgaonkar, Graham Sommer, and Chris J Diederich. Thermal therapy of pancreatic tumours using endoluminal ultrasound: Para-

metric and patient-specific modelling. *International Journal of Hyperthermia*, 32(2):97–111, 2016.

[10] Margarethus M. Paulides, Paul R. Stauffer, Esra Neufeld, Paolo F. Maccarini, Adamos Kyriakou, Richard A.m. Canters, Chris J. Diederich, Jurriaan F. Bakker, and Gerard C. Van Rhoon. Simulation techniques in hyperthermia treatment planning. *International Journal of Hyperthermia*, 29(4):346–357, 2013.

[11] M J Rivera, Molina Juan A Lpez, M Trujillo, V Romero-Garcia, and E J Berjano. Analytical validation of COMSOL Multiphysics for theoretical models of Radiofrequency ablation including the Hyperbolic Bioheat transfer equation. *2010 Annual International Conference of the IEEE Engineering in Medicine and Biology*, 2010.

Publishing Agreement

It is the policy of the University to encourage the distribution of all theses, dissertations, and manuscripts. Copies of all UCSF theses, dissertations, and manuscripts will be routed to the library via the Graduate Division. The library will make all theses, dissertations, and manuscripts accessible to the public and will preserve these to the best of their abilities, in perpetuity.

I hereby grant permission to the Graduate Division of the University of California, San Francisco to release copies of my thesis, dissertation, or manuscript to the Campus Library to provide access and preservation, in whole or in part, in perpetuity.

Author Signature Date 9/8/2017